Chapter 2

Thermal transformation of core-shell wuestite-maghemite nanocubes for improving their magnetic performances

•••

2.1 Introduction

Iron oxide nanocubes (*e.g.* Fe_2O_3 or Fe_3O_4), depending on their cube-edge size, have the tendency to strongly interact in solution due to their high magnetization properties and dipole-dipole interactions.[1] This feature can make challenging to obtain stable and single nanocubes when applying any of the common water transfer procedures, such as ligand exchange or polymer coating.[2] Indeed, biological applications of nanomaterials require their stability in complex media, composed of salts and proteins that can seriously compromise the colloidal properties and thus the activity of nanoparticles not properly functionalized or agglomerated.[1] Moreover, taking into account magnetic materials, it was demonstrated how the aggregation of Fe_2O_3 nanoparticles can affect their magnetic properties and in particular hyperthermia efficiency.[3, 4] In light of this, core-shell $Fe_{1-x}O/Fe_{3-\delta}O_4$ (wuestite/magnetite) nanocubes (NCs)[5] can be interesting alternative. This core-shell configuration is less interacting compared to iron oxide nanocubes with a single maghemite/magnetite phase. Indeed, the presence of a paramagnetic core in a ferrimagnetic shell lowers the magnetization of these nanocubes compared to single-phase Fe_3O_4 nanocubes, thus helping to prevent their aggregation and to increase their colloidal stability in the organic solvent where they are synthesized. In this status they can be handled more easily and thus processed (water transfer for instance) with standard procedures for biological applications. Upon being made water stable, the following conversion into an efficient magnetic material could be driven by transformation of their core/shell structure into a single-phase material. As the colloidal stability and isolation of the particles are of greatest importance in all biomedical applications, the research focus has been turned towards liquid phase oxidation of the FeO-Fe_3O_4 nanoparticles. [6] Previously, the main way to improve magnetization and structure of these core-shell nanoparticles was mainly focused on the post synthesis annealing in organic solvent at elevated temperature.[7-10] However, the major drawback of these harsh conditions is the destabilization and agglomeration of the particles before water transfer, due to increase of the magnetic domain. This also affects their inter-particles dipole-dipole interactions that prevail after annealing. Thus, it is important to find a milder oxidation method that triggers the transformation of the core/shell nanoparticles to a single magnetic phase while preserving their colloidal stability and possibly protecting the surface bioactive ligands. In this project, it was developed a water-compatible thermal annealing process, which led to the conversion of the wustite/magnetite core-shell structure of NCs in magnetite homostructure. This phase transformation was accompanied by a concomitant increment of the heating efficiency of the materials. The distinctive feature of the here proposed annealing process, compared to the typical thermal treatment,[7-9] is that the oxidation of the core-shell $Fe_{1-x}O/Fe_{3-\delta}O_4$ nanocubes to $Fe_{3-\delta}O_4$ took place at a temperature lower than the boiling temperature of water (usually

80 °C opposed to 120- 150 °C of the methods in organic solvents). This temperature also implies that organic coating but also some small bioactive molecules (*e.g.* folic acid) may preserve their functionalities. According to mild annealing treatment concept, *Sun et al.*[11] demonstrated the controlled oxidation of core-shell wuestite/maghemite nanocubes in a temperature range of 60-120 °C. However, at very mild condition (60 °C), they could only obtain a partial oxidation of the wuestite core and just at 120 °C the oxidation was more efficient.[11] Moreover, since the aim of the authors was to demonstrate the possibility to tune the phase transformation process, the oxidation was carried out in organic solvent, a non-relevant condition for biological applications.[11] More recently, *Lak et al.*[12] obtained the oxidation of the $Fe_{1-x}O$ core into $Fe_{3-\delta}O_4$ by applying magnetic hyperthermia (MH) in aqueous solution, in extremely mild conditions with a maximum temperature below 37 °C.[12] Moreover, they also functionalized the nanocubes with a Gallic-PEG[13] derived biotin, demonstrating the ability of the molecule to bind streptavidin even after the MH cycles.[12] However, in term of heating efficiency, the final oxidized nanocubes showed modest SAR values. As hypothesized by the authors, the presence of antiphase boundaries (APBs) at the interface of growing magnetic domains, even after thermal annealing, could be a plausible reason for the low heating performances.[7, 12, 14] In the here presented work, the core-shell nanocubes were transferred in water *via* polymer coating protocol and PEGylated in order to stabilize the nanoparticles against the thermal treatment. Compared to the work presented by *Lak et al.*[12], the oxidation process here occurred at harsher conditions, which affected the colloidal stability of NCs if some expedients were not adopted. PEGylation prior to the thermal treatment demonstrated to prevent the aggregation of NCs and an ultracentrifugation step just after the annealing, led to extremely stable nanocubes. Thermal oxidation efficiently promoted the FeO to Fe_3O_4 transformation of the NCs core, with significant increase of their magnetic properties. In particular, the interesting SAR values obtained made the nanocubes suitable for an effective hyperthermia application. Furthermore, the functionalization of the material with a folic acid as bioactive molecule, the activity of which was preserved even after the annealing, found promising application in magnetic cancer cells sorting. Noteworthy, this project can be considered a sort of continuation of the work of *Lak et al.*,[12] moving mainly toward a biological approach for developing this core-shell nanocubes system, rather than focusing on its magnetic characterization. The trick to first process the surface functionalization of the NPs and then convert them in more efficient heat mediator was the main purpose. Here, after obtaining more performing magnetic NPs functionalized with folic acid (FA), the application in magnetic cells sorting, as described in first chapter, was also explored.

2.2 Results and discussion

2.2.1 Water transfer of core-shell wuestite/maghemite nanocubes (csNCs)

Water transfer of single core-shell nanocubes was carried out *via* polymer coating technique, following an established procedure in our group.[15-17] This method relies on the use of the amphiphilic polymer poly(maleic anhydride-*alt*-1-octadecene, molar mass of 30'000 -50'000 g/mol). Exploiting the affinity of the side alkyl-chains of the polymer to the alkyl surfactant on the nanocubes, after mixing in chloroform the polymer and the nanocubes, the solvent was slowly removed using a rotavapor. Afterwards, by addition of water and a sonication step, the nanocubes were re-dissolved in borate buffer. Borate buffer (pH = 9) promoted the hydrolysis of the maleic anhydride rings, which rapidly occurs in basic solutions.[17] Under these conditions, the hydrophilic moieties of the polymer on the surface of the nanoparticles were exposed towards the solution, leading to soluble and stable NCs. At the same time, the presence of carboxylic groups of the polymeric shell, derived from maleic anhydride rings opening, offer the possibility of further functionalization with, *e.g.*, amines *via* EDC (1-Ethyl-3-(dimethylaminopropyl)carbodiimide) coupling chemistry. DLS data (**Figure 1a**) shows stable and monodisperseed (PDI = 0.081), core-shell nanocubes, with no trace of aggregation in aqueous phase, as confirmed by d_h of 35 ± 5 nm). Electrophoresis gel picture for PC-csNCs shows that the nanocubes were stable presenting a narrow migration band. This result was in accordance with the previous indicating that the nanocubes were monodispersed in size and had low tendency to aggregate. Moreover, the absence of the polymer band indicates that the sample was free of polymeric material in excess (**Figure 1b**).

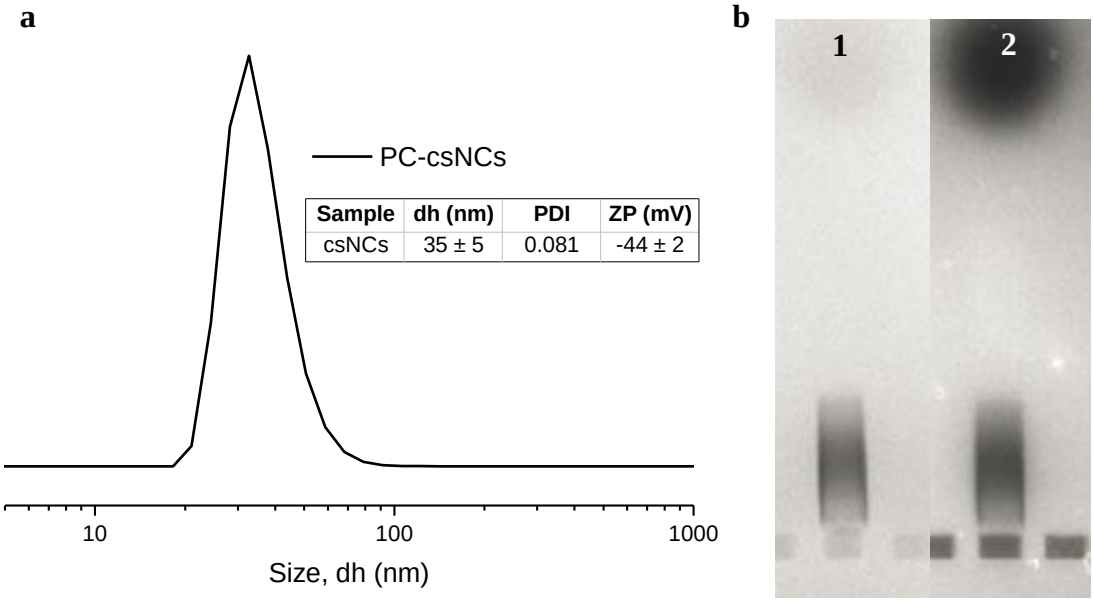

Figure 1. **PC-csNCs characterization**. **a)** Number weighed hydrodynamic diameter of core-shell nanocubes transferred in water by polymer coating procedure. Table in the inset reports the obtained hydrodynamic diameter (dh), polydispersity index (PDI) and zeta-potential (ZP). **b)** Gel electrophoresis of PC-csNCs on an agarose gel 1%. The pictures were acquired under white light (1) and under UV light (2) with a 430 nm filter, the latter in

order to detect the presence of free polymer. The black spot at the top of the gel (2) is due to the presence of orange g solution, used for making heavier the sample and trace the migration.

The strong negative charge of nanocube surface contributes to their stability, providing monodispersed polymer-coated nanocubes, as confirmed also by TEM (**Figure 2a** and **b**). Even after the water transfer the typical core-shell structure is still evident under TEM (Figure 2b)

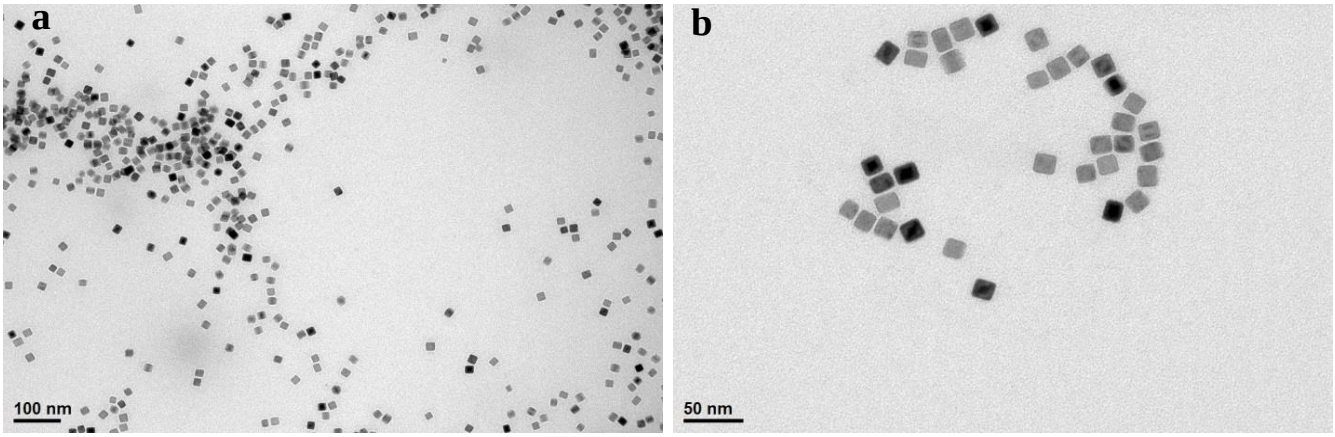

Figure 2. TEM micrographs. a) PC-csNCs after water transfer. **b)** Magnification of PC-csNCs.

2.2.2 Thermal annealing of the core-shell nanocubes

Once transferred in water, core-shell nanocubes (from now on, PC-csNCs will be referred simply as csNCs) were annealed at 80 °C for 12 h to promote the oxidation of the wuestite core (FeO) to magnetite (Fe_3O_4). Soon after the treatment, stability of the nanocubes was compromised. Indeed, DLS analysis revealed the presence of large aggregates in the sample oxidized at 80 °C for 12 h, with a drastic size and polydispersity increase (from 33 ± 1nm before annealing to 72 ± 20 nm after annealing, **Figure 3a**). Moreover, after few days the annealed sample irreversibly aggregated and precipitated at the bottom of the vial (**Figure 3b**). These data clearly indicated that the thermal process affected the colloidal stability of the NCs suspension. As previously explained, one reason could have been the increasing of the magnetic core of the nanocubes upon the oxidation process, which promoted the inter-particles interactions.[12] Another possible explanation for the stability loss at this temperature could be the loss of hydrogen bonds between the nanocubes surface and the water molecules. Indeed, one parameter to be considered when the temperature increases from room temperature (*i.e.* 20-25 °C) to 80 °C is the decrease of the water dielectric constant (ε_r), which drops from 80 to 55.51 (@ 100 °C).[18] The decrease of ε_r determines an increase of the unfavorable desolvation free energy ($\Delta\Delta G_{dslv}$) of colloidal solutions of molecules like proteins and nanoparticles. Considering the equation (1)

$$\Delta\Delta G_{tot} = \Delta\Delta G_{dslv} + \Delta\Delta G_{brd} + \Delta\Delta G_{nps} \qquad (1),$$

where $\Delta\Delta G_{tot}$ is the total electrostatic energy between solvent and nanoparticles, $\Delta\Delta G_{brd}$ is the free energy due to the inter-nanoparticle interactions of charged groups and $\Delta\Delta G_{nps}$ is the residue free energy of these interactions with the rest of the nanoparticles.[18] When T increases and the dielectric constant drops, the interactions between solvent and nanoparticles diminish and the free energy ($\Delta\Delta G_{dslv}$) increases.

Analogously, also the other free energy terms ($\Delta\Delta G_{brd}$ and $\Delta\Delta G_{nps}$) increase for the nanoparticles, due to the electrostatic repulsion between the negatively charged carboxylic groups of the polymeric shell. Consequently, the total free energy ($\Delta\Delta G_{tot}$) increase causes instability of the colloidal system.

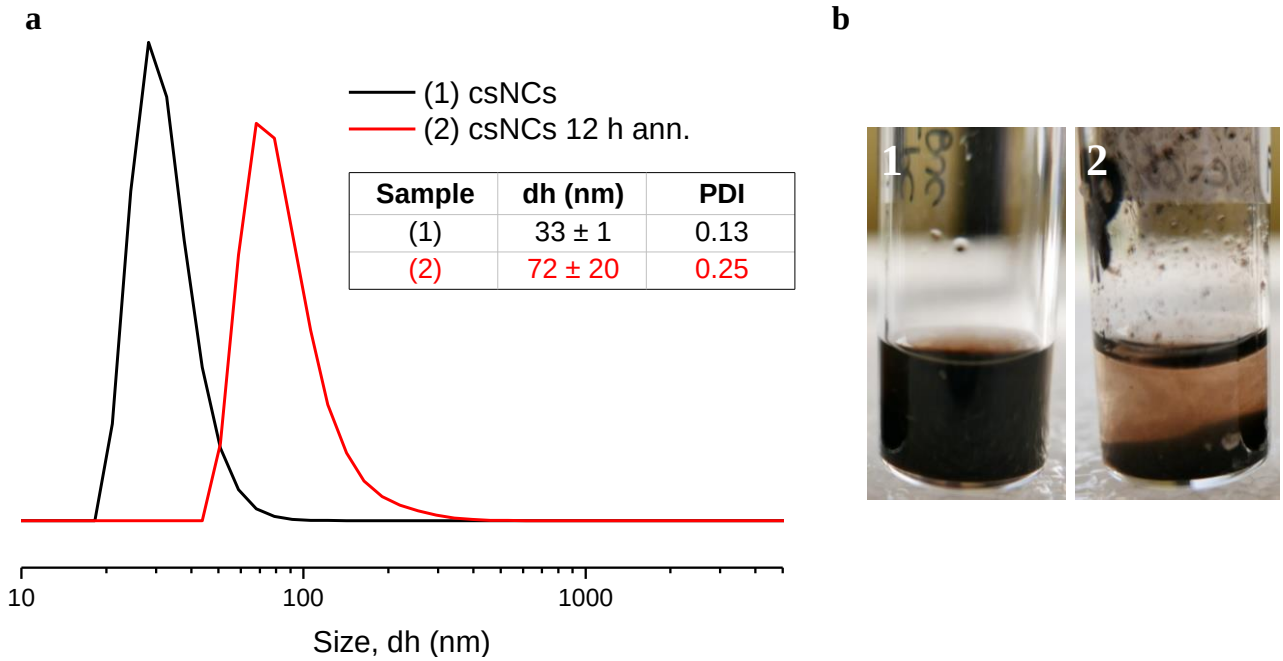

Figure 3. csNCs annealed characterization. a) Number weighed hydrodynamic diameter of core-shell nanocubes before (black line) and after (red line) thermal annealing for 12 h. Table in the inset reports the obtained hydrodynamic diameter (dh), polydispersity index (PDI). **b)** Pictures of the PC-csNCs sample before annealing (1) and after thermal treatment (2).

Thus, it was decided to introduce on the nanocubes surface PEG molecules that can increase the thermal stability of colloidal materials by steric repulsion. [19-21]

2.2.3 Functionalization of csNCs

The PEGylation reaction was done by incubating the nanocubes with EDC for 10' in a mixture of water and borate buffer 3:1. Then, amine-PEG-carboxy (Mn = 3000 g/mol) was added and the mixture let to react for 4 h. The nanoparticles were washed five times with borate buffer. DLS suggested a successful functionalization (**Figure 4a**), with an increase in hydrodynamic diameter from 35 ± 0.7 nm to 39 ± 0.9 nm. Moreover, PDI value of 0.1 indicates that the sample is monodispersed and stable. Gel electrophoresis (**Figure 4b**) indicates that PEGylation occurred by the different migration shift of csNCs_PEG (2) with respect to csNCs (1).

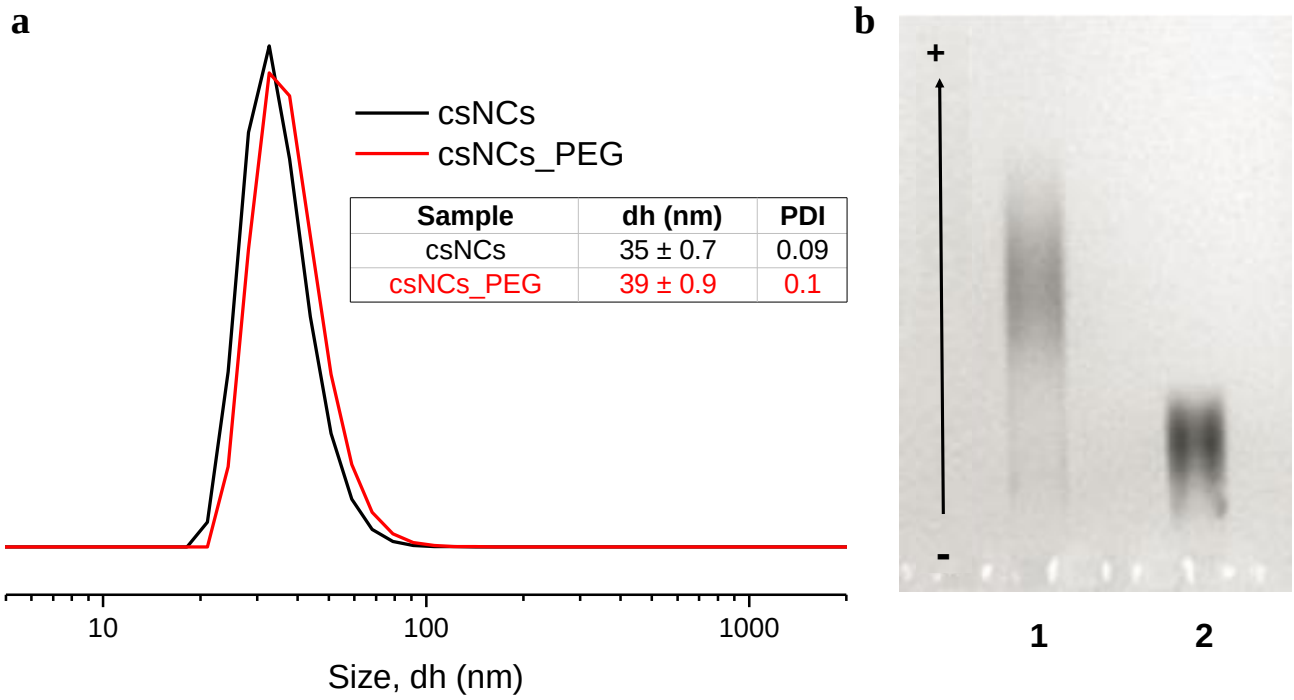

Figure 4. **csNCs_PEG characterization**. **a)** Number weighed hydrodynamic diameter of csNCs (black line) and csNCs_PEG (red line). The table in the inset shows the corresponding size and PDI values. **b)** Gel electrophoresis on a 1% agarose gel of csNCs (1) and csNCs_PEG (2).

Once found the conditions for efficiently functionalizing the nanocubes, it was possible to assess if the presence of PEG could have increased the thermal stability of the nanoparticles, as previously hypothesized.

2.2.4 Magnetic and structural characterization of csNCs

The PEGylated nanocubes were annealed at 80 °C for 12 h as for the polymer coated csNCs and in this case no aggregation occurred for the PEGylated sample after annealing (**Figure 5**). The slight difference observed in hydrodynamic size and especially for PDI, before and after thermal oxidation, could not be related to significant instability of the nanocubes colloidal suspension.

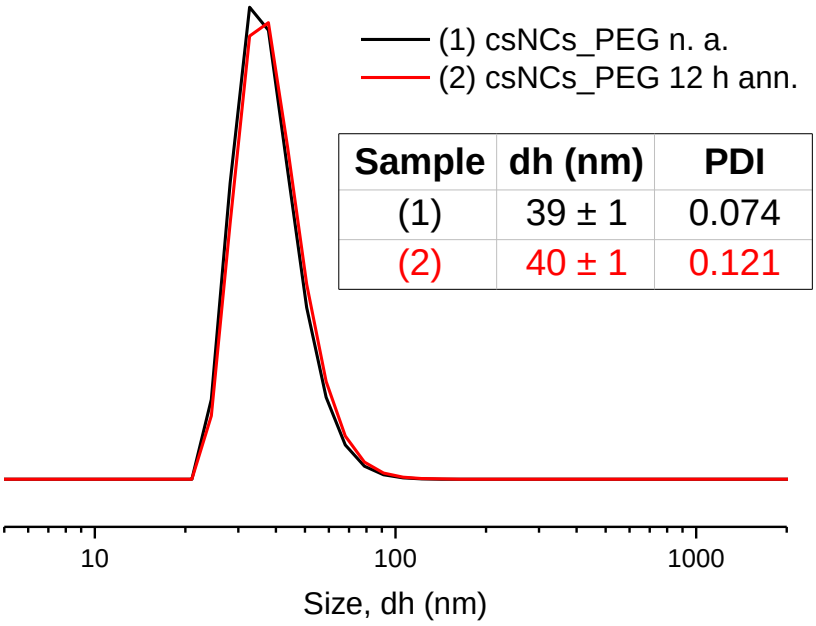

Sample	dh (nm)	PDI
(1)	39 ± 1	0.074
(2)	40 ± 1	0.121

Figure 5. Hydrodynamic size after thermal treatment. Number weighed hydrodynamic diameter of the sample csNCs_PEG. Non-annealed sample (black line) and sample annealed for 12 h (red line) are plotted. The corresponding size and PDI values are shown in the table.

Since the nanocubes were stable after annealing, it was decided to increase the incubation time up to 36 h in order to increase the csNCs heating performance measured *via* hyperthermia. Noteworthy, before measuring SAR, it was important to exclude the presence of aggregation inside the sample that is known to affect the heating properties of the nanocubes.[1, 3, 4] This point emphasizes the importance of PEG stabilizing effect during annealing (**Figure 5**). SAR values were measured by exposing the csNCs in water solution to an alternating magnetic field generated by a coil inside a commercially available device (DM100 Series, nanoScale Biomagnetics Corp.). The measurements were collected at a frequency of 301 and 105 kHz using a magnetic field of 24, 20, 15 and 12 kAm^{-1}. A non-annealed sample was analyzed as a control. The graphs in **Figure 6** show the increment of the SAR values at the different annealing times. The non- annealed sample shows a very modest SAR value, without following a linear rise with the increase of the magnetic field strength. This behavior was expected due to the presence of wuestite that presents a paramagnetic spin configuration at room temperature.[12] However, significant increase of the SAR was recorded already after 12 h of annealing, which became even more important after 36 h of thermal treatment thus indicating that the transformation of wuestite to magnetite was still taking placed after 36 h. Noteworthy, the SAR increase was proportional to the magnetic field applied, as expected for maghemite/magnetite superparamagnetic nanoparticles.[22] The highest value obtained at 301 kHz and 24 kAm^{-1}, after 36 h of annealing, was 388 W/g.

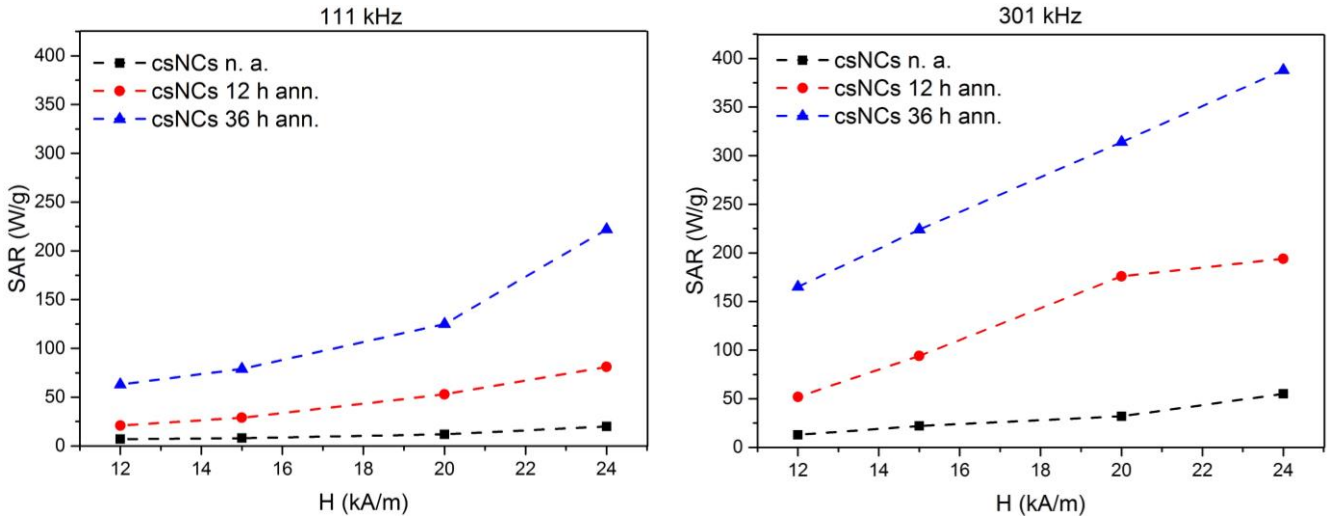

Figure 6. **csNCs SAR properties**. SAR vs Field (H) plot of csNCs_PEG obtained at the frequencies of 105 kHz **(left)** and 301 kHz **(right)**. In black are plotted the values obtained for sample non-annealed (csNCs n. a.), in red the values for the sample annealed for 12 h (csNCs 12 h ann.) and in blue for sample annealed for 36 h (csNCs 36 h ann.).

Thus, from the obtained data it was possible to conclude that the annealing at 80 °C improved the heating properties of the nanocubes. This improvement was most likely due to a structural change of the crystalline phase of the nanocubes. To confirm this hypothesis, X-Ray Diffraction (XRD) analysis was performed on the csNCs-PEG before annealing and after 12 h and 36 h of thermal treatment, in order to monitor the conversion of the core-shell wuestite/magnetite to the homostructure magnetite. **Figure 7** shows the XRD pattern obtained for the non-annealed pristine sample (black line) and for the annealed sample (12 h and 36 h) (red and blue lines, respectively). All the three samples revealed distinct and sharp diffraction peaks, indicating that they were composed by a well-defined crystalline structure. Before annealing, a biphasic crystalline structure could be observed showing the peaks from both magnetite (brown) and wuestite (gray) phases. The portion of wuestite inside the crystalline structure of the nanocubes was estimated to be ca. 40% (w/w% wuestite/maghemite, taking into consideration 311 and 111 peaks and using semi-quantitative line profile fitting). After 12 h (red line) of thermal annealing, the peaks of wuestite (111, 200 and 220) were clearly less pronounced and after 36 h (blue line) almost all the wuestite was converted to magnetite (wuestite ca. 10%, w/w%).

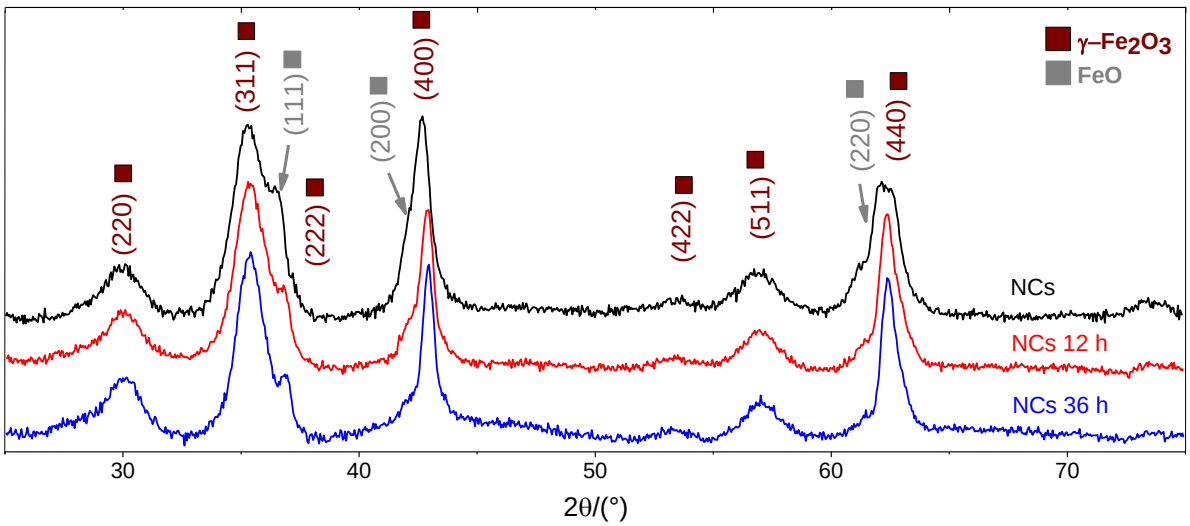

Figure 7. **XRD characterization**. csNCs before thermal treatment (black line) and after annealing at 80 °C for 12 h (red line) and 36 h (blue line).

Furthermore, XRD data demonstrate that the stability problems for csNCs (non- PEGyated) came indeed from the thermal treatment process, as initially hypothesized, and not from the magnetization increase of the nanocubes. In fact, after 12 h just a partial oxidation was observed (**Figure 7**, red line), which could not explain the high aggregation phenomenon occurred (**Figure 3**).

2.2.5 Stability issues of the annealed nanocubes

Once confirmed the transformation from a biphasic wuestite/magnetite crystalline structure to a almost complete magnetite homostructure, the aqueous stability of the nanocubes was studied in order to prove that the thermal treatment did not impair nanoparticle stability. Thus, DLS analysis was performed after annealing. As clearly visible from the results in **Figure 8**, particles are stable and homogeneously distributed. However, a decrease in size occurs for nanocubes heated for 36 h, with the dh which decreases from 39 ± 1 nm to 32 ± 1 nm. This result could be related to the polymeric shell loss. To confirm this hypothesis, further characterizations were performed.

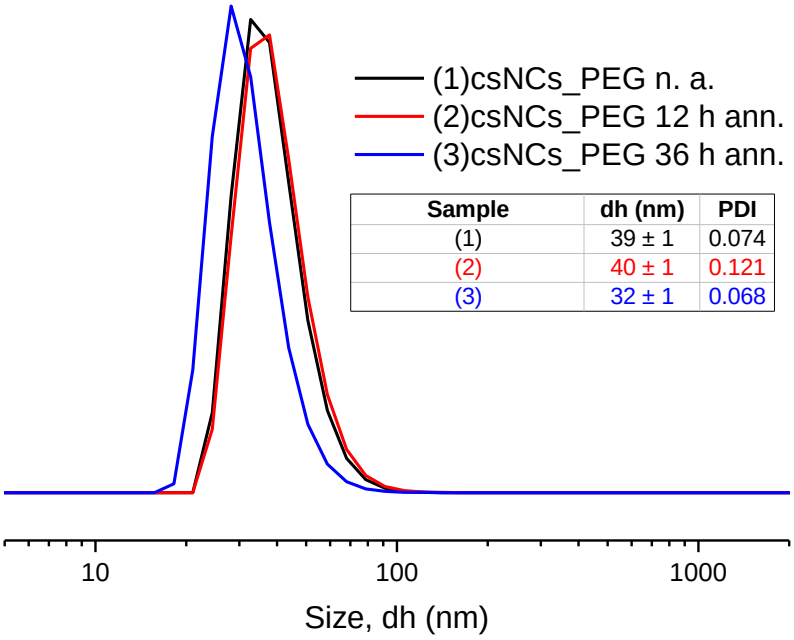

Figure 8. **Hydrodynamic size after thermal treatment.** Number weighed hydrodynamic diameter of the sample csNCs_PEG. Non-annealed sample (black line), annealed for 12 h (red line) and for 36 h (blue line). The corresponding size and PDI values are shown in the table.

Electrophoresis on agarose gel was carried out in order to monitor the migration pattern of the nanocubes after different annealing conditions. From the gel picture in **Figure 9**, the different migration of PEGylated nanocubes (**2**) and pristine sample (**1**) is evident. After 12 h and 36 h of thermal annealing, the migration pattern is consistent with the loss of polymer and PEG molecules, from the particles. This phenomenon is visible in Figure **7b**, which shows the gel under UV light (red squares).

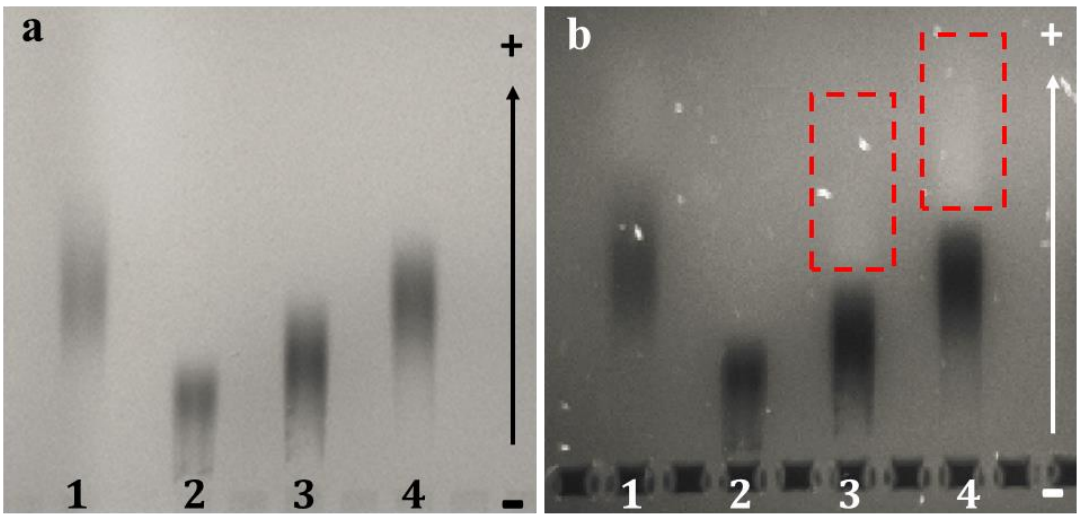

Figure 9. Electrophoresis characterization. csNCs (**1**) and csNCs_PEG (**2**) at 12 h (**3**) and 36 h (**4**) of annealing. The gel pictures were acquired under white light **a)** and under UV light **b)** using a 480 nm filter. Run was carried out on a 1% agarose gel.

In order to investigate the consequences of the detected polymer loss on the stability of the nanocubes, DLS measurements in saline solution at different concentrations were carried out. Indeed, PEG coating provides a higher stability of the nanoparticles in the presence of high salt concentration as confirmed for the non-annealed sample (black line in graph of **Figure 10**). The size of csNCs_PEG annealed for 12 h and 36 h increases already at a concentration of 0.5 M of salt (red and blue lines), indicating that the polymeric shell and consequently the PEG coating were compromised during the thermal treatment, resulting in severe instability of nanocubes in saline solution. Indeed, from **Figure 10** it is also possible to notice that longer annealing processes led to a samples less stable at higher salt concentrations.

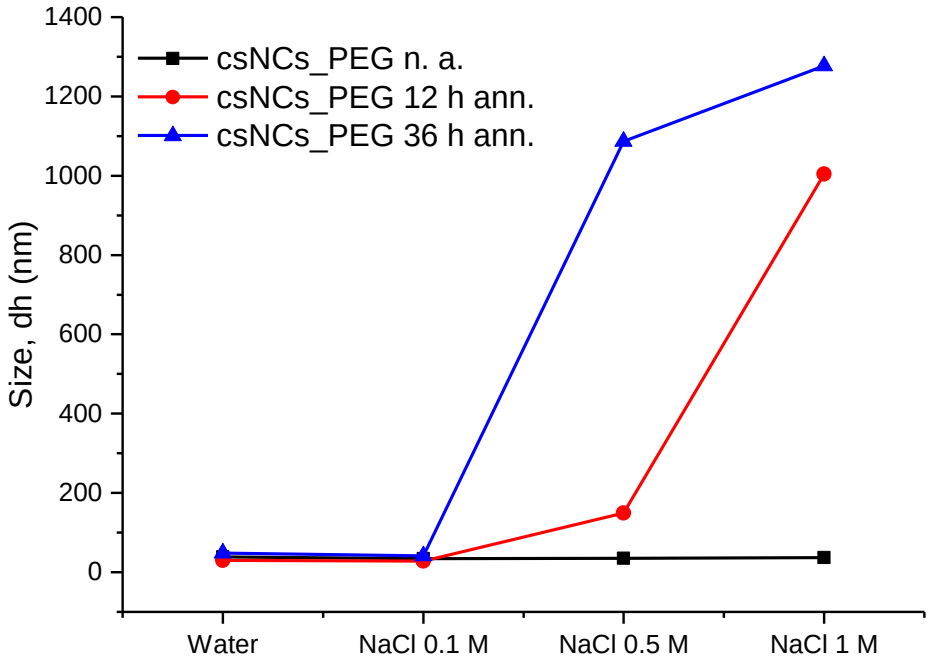

Figure 10. **csNCs after annealing: stability at different concentration of NaCl**. Size values of the nanocubes plotted against the saline solution at different concentrations. Non-annealed sample (black line), annealed for 12 h (red line) and for 36 h (blue line).

Besides the loss of stability of the thermal treatment, it seems that annealing induces also the cleavage of the polymer from the particle surface. This leads to a reduced stability if the treatment is performed for longer periods (36 h). Therefore, it is reasonable to assume that this loss might be related to the polymer weakly bound to the nanocubes. In order to try to solve this issue the polymeric shell of the nanocubes was crosslinked with 2,2′-(Ethylenedioxy)bis(ethylamine) (EDBE), as shown in **Figure 11**. This strategy is similar to that shown in chapter 2 but was done on single nanocubes after the water transfer. Three different reactions were set, varying the amount of EDBE molecules per nanoparticle (**Figure 11**, **Table 1**).

Table1. EDBE molecules amount used for each crosslink reaction

Sample	EDBE molecules
1	1100
2	500
3	250

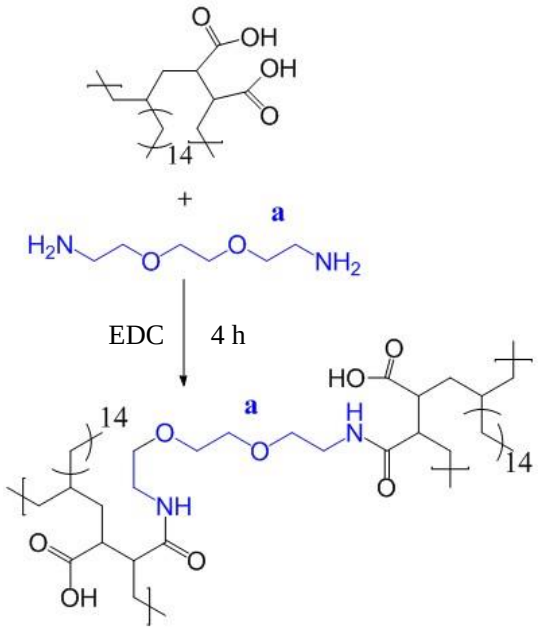

Figure 11. Crosslink reaction. Scheme of the reaction between the amines group of EDBE and carboxylic groups of poly(maleic anhydride-alt-1-octadecene), via EDC chemistry. **Table 1** reports the amount of molecules used for each reaction.

EDBE was then reacted with nanocubes after the activation of the carboxylic groups of the polymer *via* EDC (128,000 molecules/NCs) for 10 minutes. The solution was let to react for 4h. After five washes, the nanoparticles were functionalized with amine-PEG-carboxy (1000 molecules/NCs) *via* the EDC chemistry. The nanocubes were then washed (five times), recovered and annealed at 80 °C for 12 h and 36 h. Subsequently, electrophoresis was carried out on a 1% agarose gel. **Figure 12** shows the migration pattern of the csNCs before crosslinking (A), after EDBE addition (EDBE 1/2/3), after PEGylation (PEG 1p/2p/3p) and after annealing treatments (12/36 h ann., 1p/2p/3p). Despite the presence of the cross-linker molecule, the migration pattern of the PEGylated samples drastically change after annealing, assuming the profile of the non-PEGylated nanocubes. Due to the high concentration of crosslinker, which may provide higher stability to the polymeric shell, the sample of csNCs_1 showed less migration with respect to csNCs_2 and 3 (after 12 h annealing and 36 h of thermal treatment). However, the results obtained were similar to the ones obtained and showed in **Figure 9** without crosslinker, indicating the lack of stability of the polymeric shell. It was possible to conclude that the addition of a cross-linker molecule was not able to prevent the miss folding events that occurred at the polymeric shell surface of the csNCs.

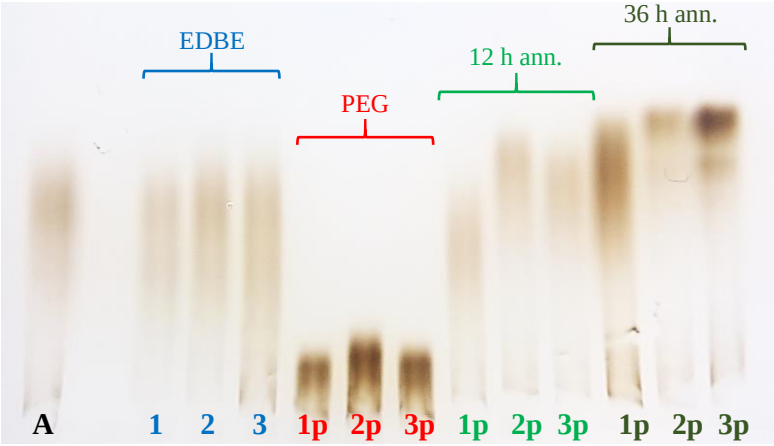

Figure 12. Electrophoresis characterization. A) csNCs pristine. **1**) csNCs_1 (EDBE 1100 molecules); 2) csNCs_2 (EDBE 500 molecules); 3) csNCs_3 (EDBE 250 molecules). 1p) csNCs_1_PEG; 2p) csNCs_2_PEG; 3p) csNCs_3_PEG. 1p, 2p and 3p after 12 h of annealing. 1p, 2p ad 3p after 36 h of annealing. Run was carried out on a 1% agarose gel.

As further confirmation of the outer polymeric shell loss/PEG loss, the three samples were incubated in NaCl 1 M solution. As shown in **Figure 13**, while csNCs_1/2/3 PEGylated are stable and monodispersed both in water and high salt concentration before annealing (**Figure 13a,** blue lines), after thermal treatment of 12 h (light green line) and 36 h (dark green lines) the three samples strongly aggregated at high salt concentration (**Figure 13b**, **13c** and **13d**).

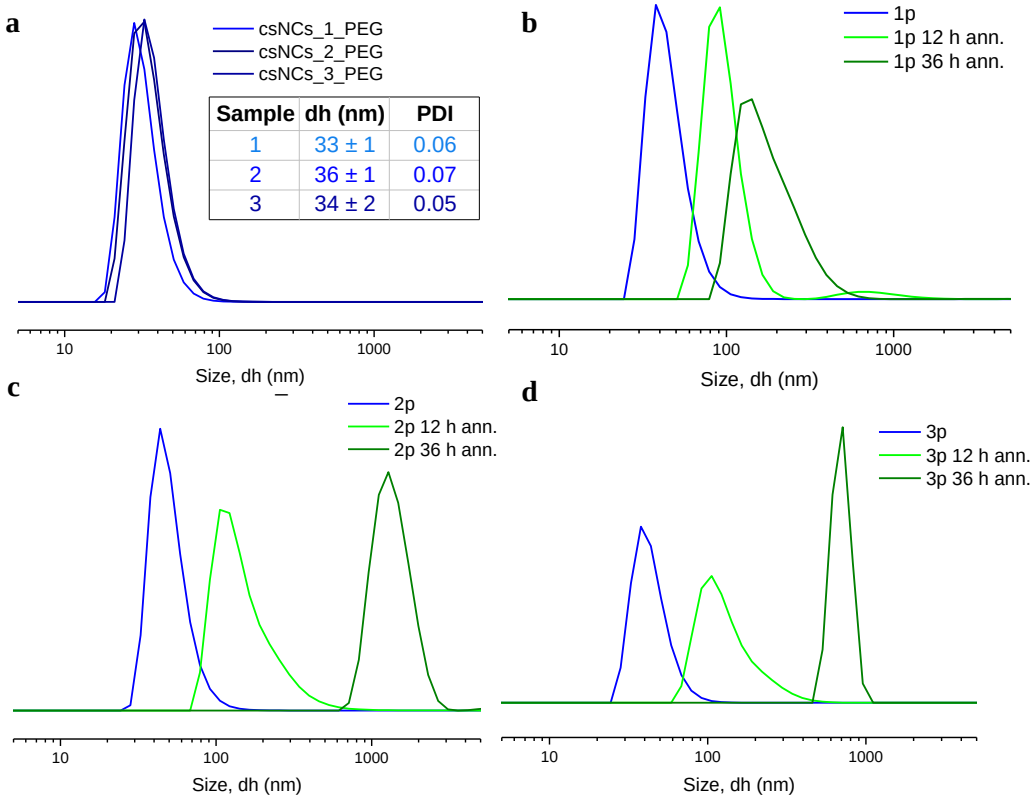

Figure 13. Hydrodynamic size of crosslinked csNCs. a) Number weighed hydrodynamic diameter of the three samples csNCs_1/2/3 in water. **b)**, **c)** and **d)** Number weighed hydrodynamic diameter of csNCs_1/2/3_PEG,

respectively, before thermal treatment (blue line) and after 12 h (light green line) and 36 h (dark green line) of annealing.

These results clearly show that the crosslinking strategy relying on the used of EDBE molecule is not a suitable option to improve the csNCs stability upon annealing treatment. Instead, the results obtained were similar to those showed in **Figure 10**. Thus, to efficiently improve the stability of the material under the thermal process, it was designed a new protocol. A double functionalization strategy was developed, as depicted in **Figure 14**. After a first PEGylation step (**1**), the nanocubes were annealed at 80 °C (**2**). Then, the nanoparticles were purified by ultracentrifugation at 20,000 rpm for 40 minutes using a sucrose gradient (20%-40%-60%) in order to remove the weakly bounded polymeric layers detached after thermal treatment (**3**). Once recovered, the nanocubes were further PEGylated with PEG-FA shown in chapter 1 (**4**) and annealed for further 36 h (**5**).

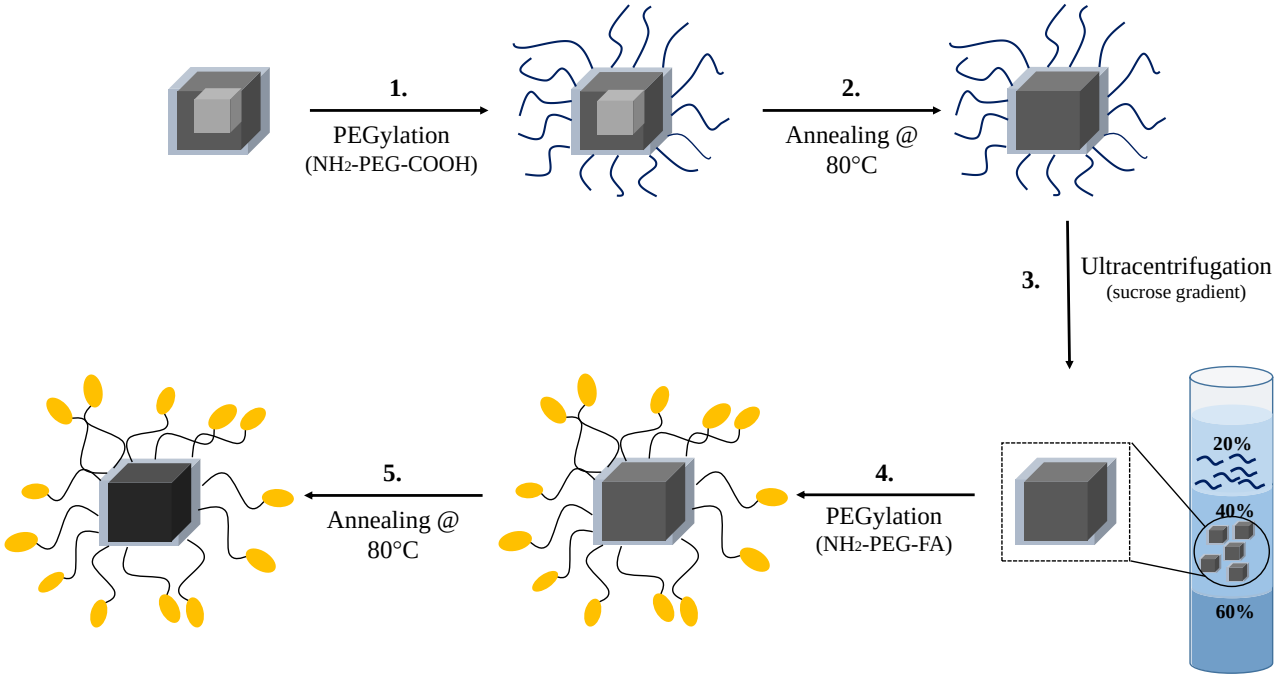

Figure 14. **Schematic representation of the new developed procedure for the functionalization and annealing of core-shell iron oxide nanocubes. (1)** The nanocubes were PEGylated and annealed @ 80 °C for 36 h **(2)**. Then, the sample was purified via ultracentrifugation at 12,000 rpm for 40 minutes on sucrose gradient (20%-40%-60%) **(3)**. the nanocubes were then PEGylated with PEG-FA (**4**) and annealed for further 36 h (**5**).

After each step, the nanocubes were characterized *via* DLS and gel electrophoresis. As discussed above, the annealing process determined the detachment of the outer polymeric shell layers, and thus the PEG, from the nanocubes surface, resulting in the aggregation of the particles in high salt solution (NaCl 1M). However, the introduction of a second PEGylation step, even if it is followed by another cycle of thermal annealing, resulted in highly stable nanocubes in saline solution (NaCl 1M). DLS graph in **Figure 15** shows the hydrodynamic size profiles of the PEGylated nanocubes after the ultracentrifugation, before and after the second thermal annealing. The nanocubes kept their stability unchanged after the second

heat treatment, and the size of csNCs_PEG before (34 ± 1 nm) and after annealing (35 ± 1 nm) were comparable.

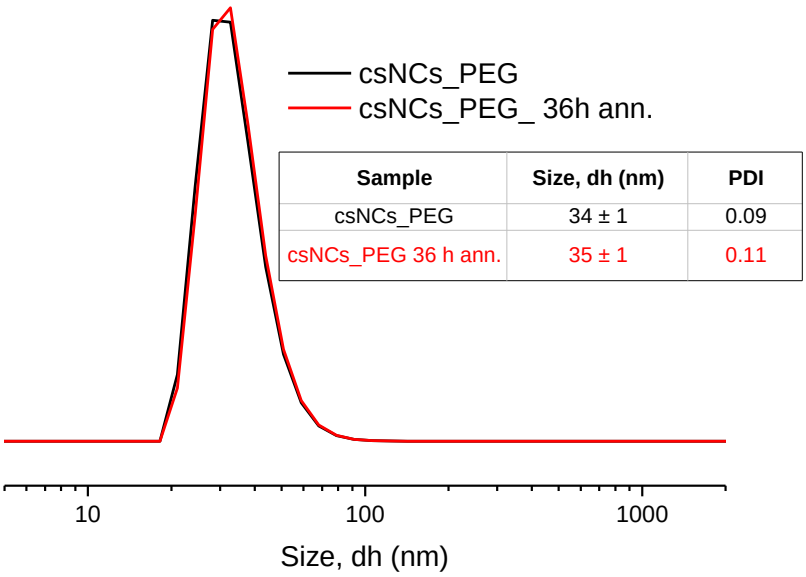

Sample	Size, dh (nm)	PDI
csNCs_PEG	34 ± 1	0.09
csNCs_PEG 36 h ann.	35 ± 1	0.11

Figure 15. Stability test in NaCl 1 M. Number weighed hydrodynamic diameter of the sample PEGylated for the second time, in NaCl, before and after the annealing (36 h). The corresponding size and PDI values are shown in the table.

Furthermore, gel electrophoresis (**Figure 16**) not only confirms the stability of the nanocubes (line 4), which migrated throw the agarose without any sign of aggregation, but it also suggested that the polymeric shell, and thus the PEG coating, was retained on the nanoparticles surface. Indeed, the migration pattern of the sample in line 4 is similar to that of the samples in lines 1 and 3 corresponding to the stable PEGylated samples. Moreover, the picture acquired exposing the gel under UV light (**Figure 16b**) did not shown any trace of polymer migration, indicating the stability of the csNCs shell.

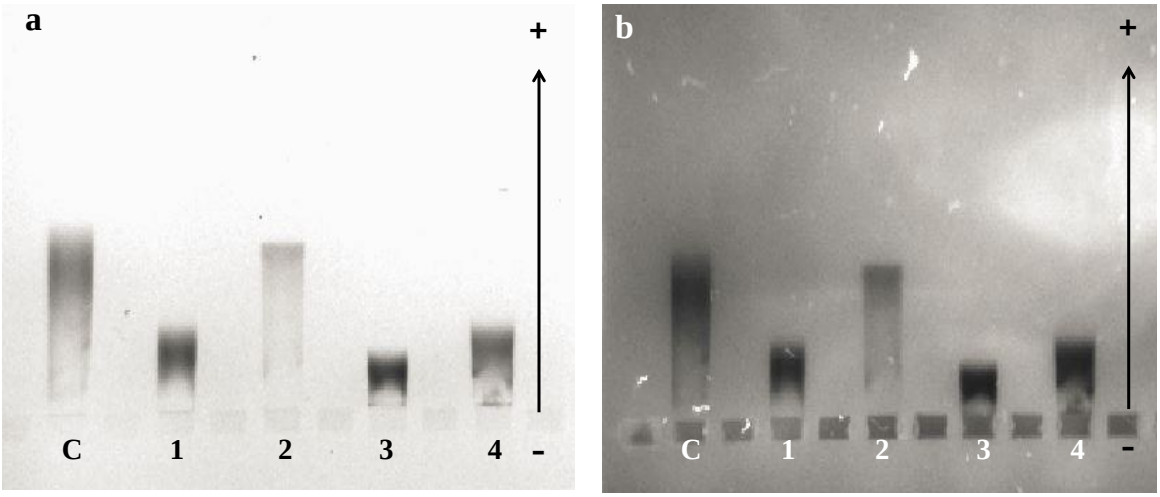

Figure 16. **Electrophoresis on 1% agarose gel**. (**C**) pristine nanocubes, (**1**) PEGylated sample, (**2**) PEGylate sample of line 1 after first annealing, (**3**) sample of line 2 PEGylated after ultracentrifugation, (**4**) sample of line 3

after 36 h of thermal treatment. The gel pictures were acquired under white light **a)** and under UV light **b)** using a 480 nm filter.

2.2.6 Magnetic and structural characterization of the nancubes @ 72 h of annealing

The thermal treatment was carried out not only for 36 h, but in this case also for 72 h. This increment of annealing time indeed could have reasonably promoted a further reorganization of the crystalline structure of the nanocubes, *e.g*. increase of the SAR value. The SAR values, measured at a frequency of 301 kHz and different magnetic field amplitudes (in the range between 15 kAm^{-1} and 24 kAm^{-1}) after the second annealing cycle showed a linear increase proportional to the strength of the magnetic field applied (**Figure 17**).[22] Interestingly, the maximum value obtained from these measurements (401 W/g) was slightly higher than the maximum value obtained after 36 h of annealing (388 W/g). To evaluate the hyperthermia performances in conditions similar to that *in* vivo, SAR measurements in high viscous media were carried out. The water-glycerol (W:Gly) mixtures were set to 64:36 v%, 32:68 v%, and 19:81 v%, corresponding to a mean η of 3.8, 24, 97.3 mPa.s respectively[23] As shown in the graph of **Figure 17**, the nanocubes SAR values dropped by increasing the viscosity of the media, as already reported by *Cabrera et al.*[23]

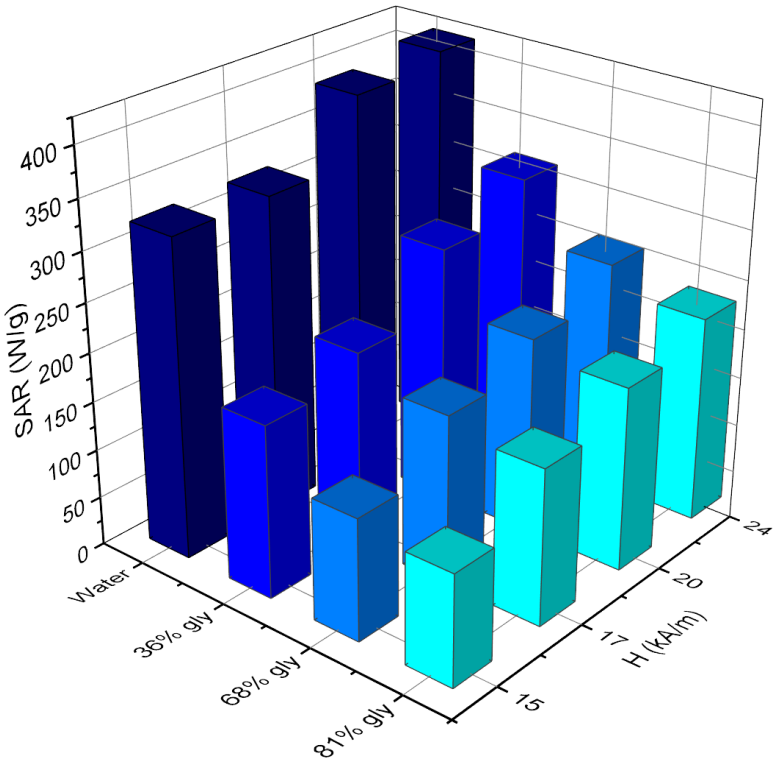

Figure 17. Specific absorption rate (SAR) characterization of csNCs at 72 h of annealing. SAR values as function of four magnetic field amplitudes (15, 17, 20 and 24 kAm^{-1}) at the frequencies of 301 kHz, measured in different viscous media (water, 81%, 68% and 36% glycerol).

The SAR values obtained in **Figure 17** are in line with those calculated and shown in **Figure 6**. Furthermore, X-Ray diffraction analysis was performed on the csNCs sample annealed for additional 36 h, in order to confirm that the transition from wuestite to magnetite was the cause of the further boost of

their hyperthermia properties. **Figure 18** shows the XRD pattern obtained for the nonannealed pristine sample (black line), for the sample annealed for 36 h (blue line) and for the sample annealed for a total of 72 h (red line). As showed in **Figure 7**, before annealing a biphasic crystalline structure could be observed showing the peaks from both magnetite (brown) and wuestite (gray) phases. After 36 h of thermal annealing, almost all the wuestite was converted to magnetite (blue line). However, the additional 36 h of annealing promote the efficient conversion of the remaining wuestite to maghemite and the peaks of wuestite (111, 200 and 220) disappeared almost completely (wuestite < 5%, w/w%).

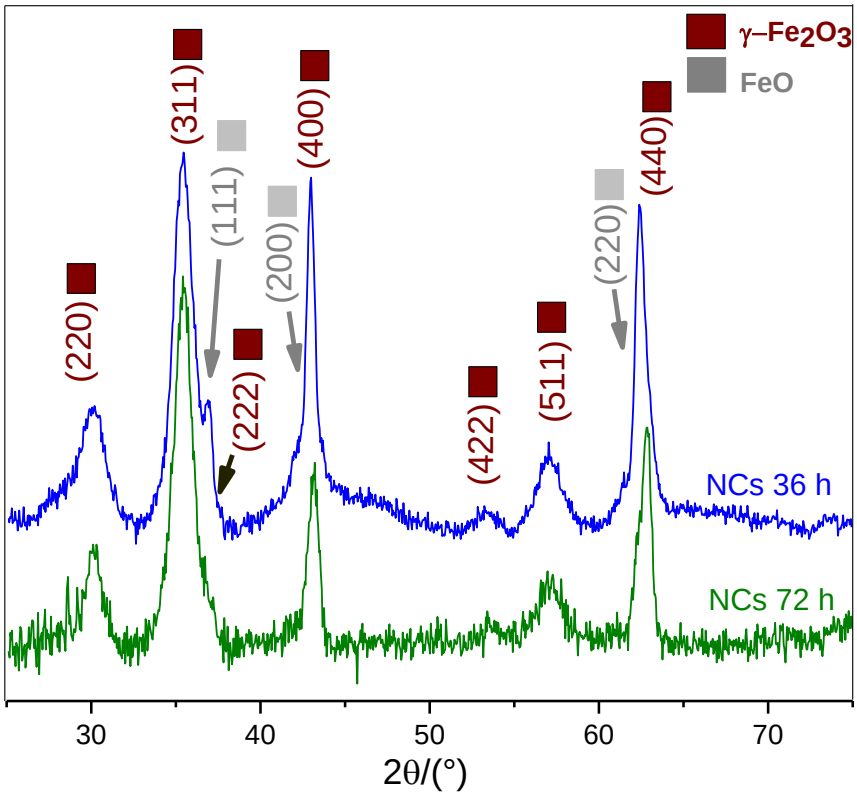

Figure 18. XRD characterization. csNCs after annealing at 80 °C for 36 h (red line) and 72 h (blue line).

From the XRD data it was possible to conclude that the increase of SAR values recorded after the additional annealing process (**Figure 17**) could be ascribed to the further FeO to Fe_3O_4 core transformation and to a deep rearrangement of the nanocubes crystalline structure.

2.2.7 Functionalization of the nanocubes with PEG-FA

The PEG-FA molecules synthesized according to the procedure reported in chapter 1 was used for the functionalization of the csNCs. CsNCs treated as reported in step (3) (**Figure 14)** were incubated with EDC for 10 minutes in a 1:3 mixture of water and borate buffer. Then, amine-PEG-FA (Mn= ~2,000 g/mol) was added and the mixture allowed to stir for 4 h. Afterwards, the washing procedure was performed five times with PBS (pH = 7.4), using an amicon (cutoff 100,000 g/mol). The functionalization was characterized *via* DLS and electrophoresis (Figure 19). CsNCs were also PEGylated with the commercial bis(amine)PEG (PEG-NH_2). This batch was done as functionalization control, since

bis(amine)PEG is the precursor of the PEG-FA synthesis. DLS results in **Figure 19a**, show a slight increase of the beads size after PEGylation. Indeed, it was reasonable to hypothesized a rolled conformation of the PEG molecules around each nanocube.[24] Nevertheless, no significant variation in the size of the beads functionalized with PEG (green line) and PEG-FA (olive line) was observed, reasonably due to the low size difference existing between the two molecules. Noteworthy, after the PEG addition, csNCs appeared stable and monodisperse, with no traces of aggregation. However, the zeta potential values (table in **figure 19a**) indicated the changing in the surface charge properties for the nanocubes after the modifications. In detail, after each step of functionalization, the negative charge of NCs surface shifted toward more positive value, due to the saturation of the negative carboxylic groups with positive charged molecules of PEG-NH_2. The addition of PEG-FA produced a charge shift back toward more negative value, due to the presence of both charged amine and carboxylic groups in the folic acid structure. A clear indication of the PEGylation events came from electrophoresis gel analysis. **Figure 19b** shows the gel picture of csNCs pristine (line 1), csNCs_PEG-NH_2 (line 2) and csNCs_PEG-FA (line 3). Migration shift is evident for both PEGylated samples and is even more delayed for csNCs_PEG-NH_2 compared to csNCs_PEG-FA, consistently with the charge difference between the two samples.

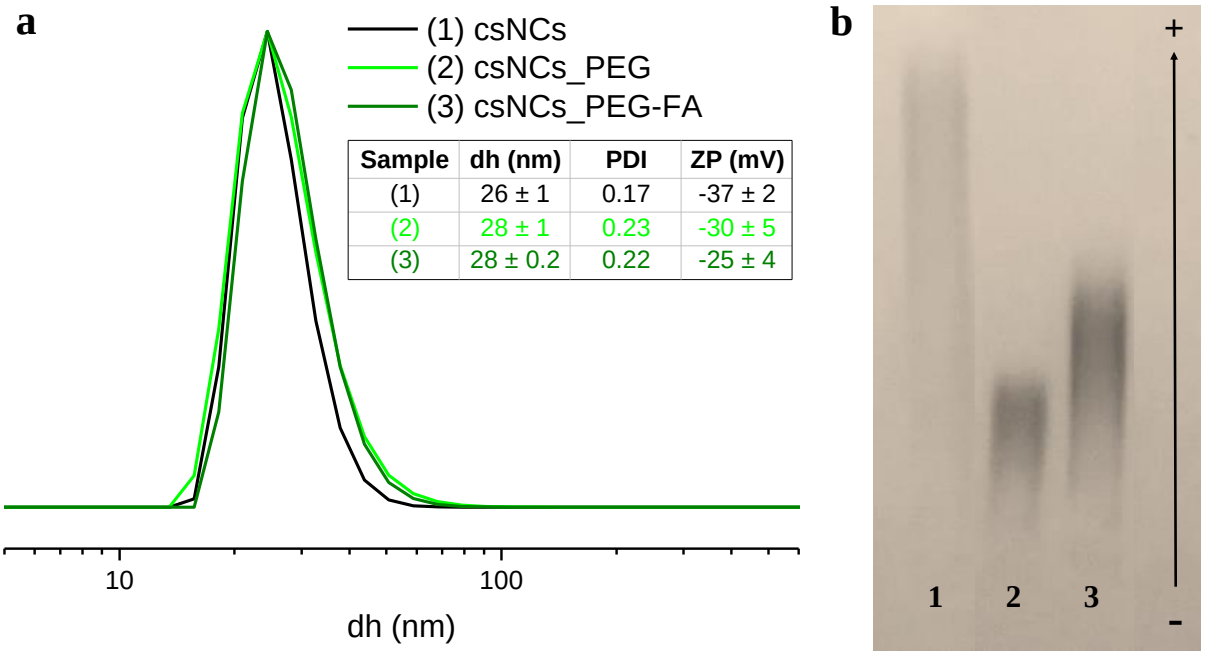

Figure 19. **Characterization of PEGylated csNCs**. **a)** Number weighed hydrodynamic diameter of the sample PEGylated with a standard bis(amino) PEG and with PEG-FA. **b**) Electrophoresis run on a 1% agarose gel, at 100 V for 40 minutes. 1 = pristine nanocubes; 2 = PEG-NH_2 sample; 3 = PEG-FA sample.

2.2.8 Stability of the nanocubes @ 72 h of annealing

Core-shell NCs functionalized with PEG-FA, were annealed for further 36 h (for a total of 72 h of thermal process, given the first annealing of 12 h) and the stability of the sample assessed in NaCl 1 M solution. This experiment was done to confirm that the nanocubes are stable at elevated temperature even with the PEG-FA. As shown in the graph of **Figure 20a**, the csNCs_PEG-FA were stable after annealing. The

values of hydrodynamic size and polydispersity are also the same (table of **Figure 20a**). Moreover, electrophoresis gel picture in Figure 20b revealed the absence of migration difference between the sample before and after annealing (lines 3 and 4). In addition, the picture acquired exposing the gel under UV light (**Figure 20c**) did not shown any trace of polymer migration, indicating the stability of the csNCs shell and reasonably also of PEG-FA functionalized nanocubes.

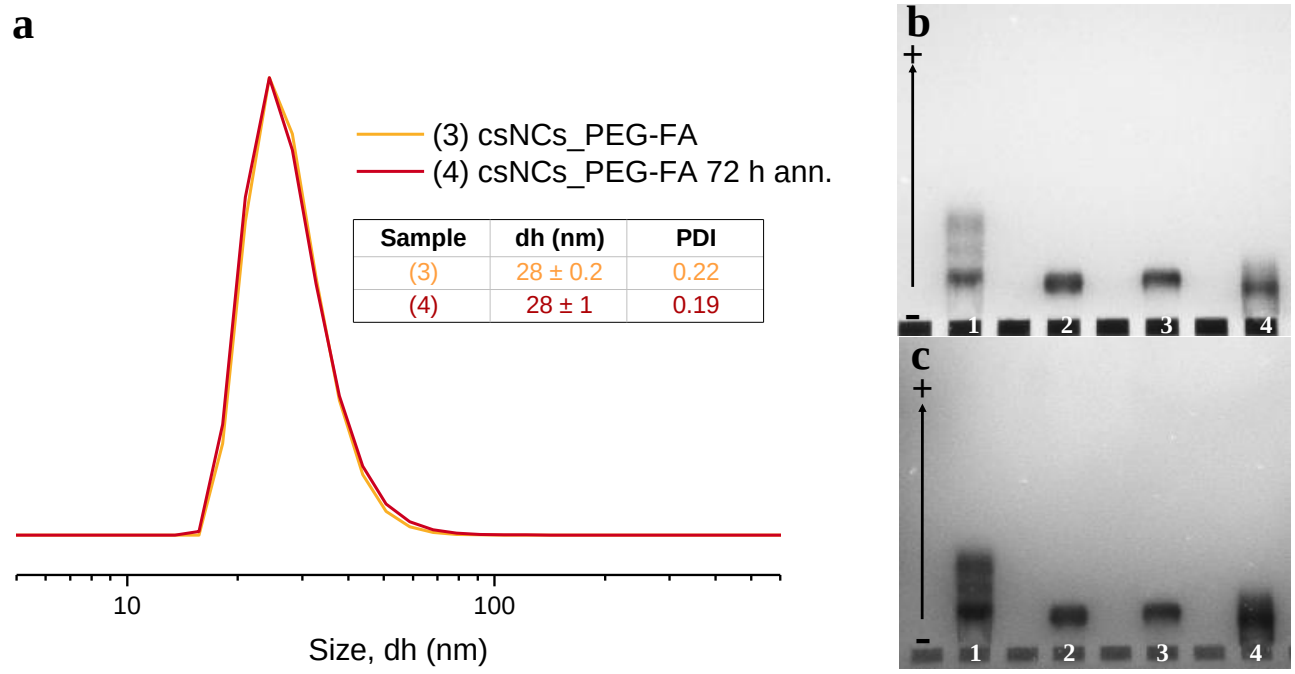

Figure 20. Characterization of csNCs_PEG-FA after annealing. **a)** Number weighed hydrodynamic diameter of the sample PEGylated with a standard bis(amino) PEG and with PEG-FA. **b)** Electrophoresis run on a 2% agarose gel, at 100 V for 40 minutes. 1 = pristine nanocubes; 2 = csNCs_PEG-NH_2 sample; 3 = csNCs_PEG-FA sample; 4 = csNCs_PEG-FA sample after further 36 h of annealing. The slight migration difference observed in this case for csNCs_PEG and csNCs_PEG-FA compared to the gel of **Figure 19** can be ascribed to the higher gel density used in this case. This can also explain the broader migration observed for sample 1, which could indicate the presence of nanocubes with slight difference in physical size.

These nanocubes were then used as nanosystems for biological application. The first observation about the annealing process was the increase of the nanocubes magnetization, *i.e.* a boost of magnetic hyperthermia (**Figure 6** and **17**). Moreover, the core-shell transformation would have reasonably promoted the conversion of the nanocubes into magnetic sorting-responsive material.

2.2.9 Cell sorting experiments: exploiting the functionalized nanocubes

Because their heating performance was sensitive to the viscosity of the medium, with possible affection on the hyperthermia efficiency on cells, the nanocubes were used for other application. csNCs_PEG-FA were tested for their ability to specifically bind the tumorigenic KB cell line (subline of the ubiquitous KERATIN-forming tumor cell line HeLa) overexpressing folate receptor (FR overexpressing cells referred as FR+). For the sorting experiment, according to the optimized procedure described in chapter 1, KB cells were incubated at 4 °C with nanocubes functionalized with PEG-NH_2 or PEG-FA for 1 h,

keeping a ratio of 1 μg of iron/50,000 cells. The nanocubes samples used were annealed for 36 h and 72 h. The aim of the experiment was not only to observe an increase of the sorting efficiency but also to prove that the annealing process did not affect the activity of folic acid. **Figure 21** shows the binding percentage of the nanocubes functionalized (csNCs_PEG-FA) or non-functionalized (csNCs_PEG) with PEG-FA and annealed for 36 h (orange bar) and 72 h (red bar). The obtained results showed a significant binding difference between the FA-functionalized and non-FA functionalized materials, revealing a much higher binding for the former, compared to that of folic acid-free csNCs. Noteworthy, the sample non-annealed was not able to efficiently sort the cells as the annealed one. However, it still showed binding specificity (as highlighted by the significant difference of the sorting efficiency (S_e) with the sample non-annealed and PEGylated without FA). Interestingly, after the second annealing treatment for 36 h (72 h annealing, red bar) the csNCs were still able to bind the target cells, indicating that thermal treatment did not affected the biological activity of folic acid.

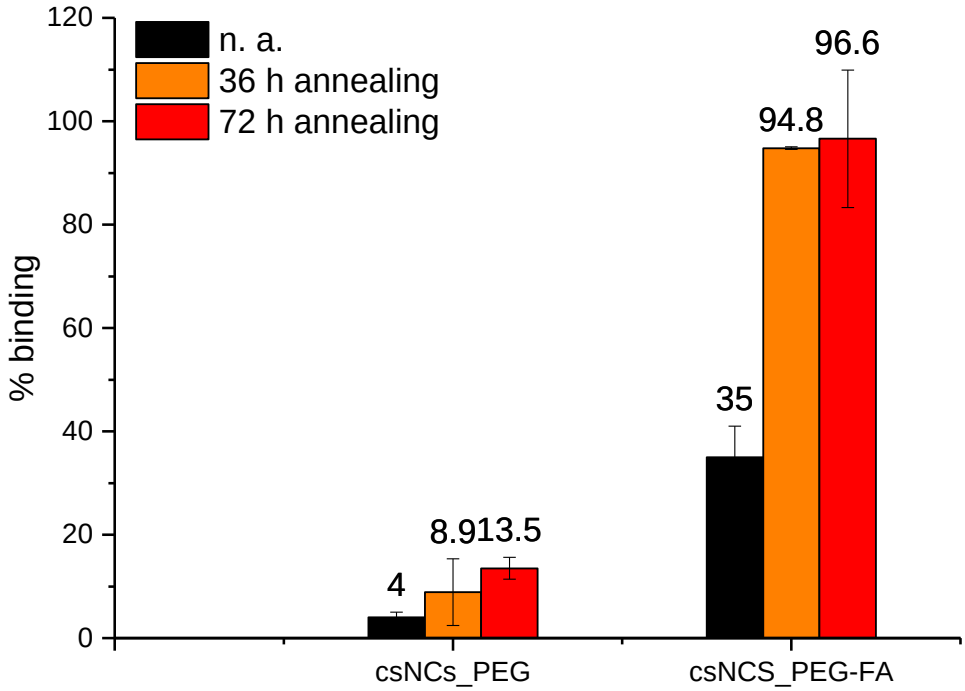

Figure 21. Sorting properties after thermal treatment. KB cells were incubated with csNCs_PEG and csNCs_FA for 1 h at 4 °C with the particles. At the end of the incubation, the cells were centrifuged, washed and collected using IMACS column. The data referred to the csNCs sample non-annealed (black bars) after the first annealing treatment (orange bars) and after the second thermal process (red bars).

In addition, elemental analysis (ICP-AES) of the iron content found in the cells after sorting was performed. The data reported in **Figure 22a** shows that the iron per cell (express as pg_{Fe}/cell) of the sample incubated with nanocubes (annealed for 36 h and 72 h) functionalized with folic acid was more than twice the amount found inside the sample treated with the non-functionalized sample. This indicates the specificity of the csNCs_PEG-FA for the target cells. Furthermore, as shown in graph of **Figure 22b**, the percentage of the iron bound to the cells, compared to the total iron used for the sorting, was significantly higher for the cells incubated with csNCs_PEG-FA than csNCs-PEG. Since just ca. 20% of the total iron (derived from csNCs_PEG-FA) incubated with the cells was found in the sorted fraction, it

is reasonable to expect to reach a significant sorting efficiency by further reducing the amount of magnetic material used. Another important evidence that emerged from these data is that the S_e is effectively dependent from the oxidation state, and thus from the magnetic properties of the nanocubes. Indeed, the amount of iron per cells (ca. 3.8 pg_{Fe}/cell for non-annealed csNCs and ca. 3.5 pg_{Fe}/cell for annealed csNCs) and the percentage of total iron (ca. 19% for non-annealed csNCs and ca. 22% for annealed csNCs) found were comparable for both csNCs_PEG-FA annealed and non-annealed (**Figure 22a**).

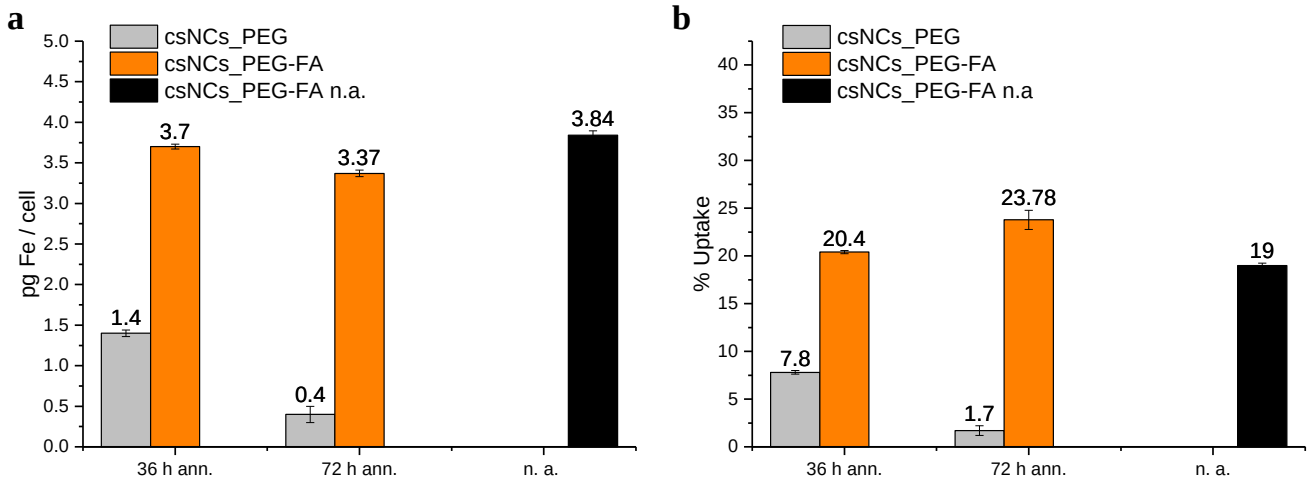

Figure 22. Characterization of the cells iron content. NCs uptake by KB cells express as pg of iron per cell **a)** and uptake percentage **b)**, relative to the total amount of iron used for the incubation, for csNCs_PEG annealed (grey bars), csNCs_PEG-FA annealed (orange bars) and csNCs_PEG-FA non-annealed (black bars). The values were normalized for the natural iron content found in non-magnetically treated cells.

2.3 Conclusion and perspectives

Due to the peculiar paramagnetic/ferromagnetic structure, which prevented the strong magnetic interactions, core-shell wuestite/magnetite ($Fe_{1-x}O/Fe_{3-\delta}O_4$) nanocubes were efficiently transferred in water using the polymer coating procedure. The thermal treatment, whose aim was the oxidation of the core and consequently the increase of the magnetic domain, was initially detrimental for the stability of the NCs. The nanocubes lost their polymeric outer shell. To solve the problem, a PEGylation step was added before annealing, considering the stability properties that PEG is known to confer to macromolecules like proteins.[19-21] As expected, the PEGylation step conferred thermo-stability to the csNCs. The annealing process efficiently promoted the conversion of the nanocubes crystalline structure from core-shell wuestite/magnetite to homostructure magnetite, thus improving the heating performances of the nanoparticles. The SAR values obtained were encouraging for exploiting this material in hyperthermia treatment. However, the nanocubes were still very unstable in saline solution after annealing. To solve the problem, a second PEGylation step was carried out after the first thermal annealing, resulting in more stable NCs in water than that after only one step of PEGylation. Interestingly, the nanocubes were stable after a further thermal treatment (rising the total thermal oxidation process up to 72 h), which also increased the heating performances of the material. However, calorimetric measurements of SAR in viscous media demonstrated the viscosity dependence of these nanocubes, resulting in a linear decrease of SAR values by increasing the viscosity of the media. Even if the absolute values were still significantly high for hyperthermia applications, thanks to the increased magnetic moment, nanocubes were here tested for magnetic sorting purpose. A second PEGylation step was performed using a PEG-FA already shown in chapter 1, for directing the nanocubes towards the FA expressing cells. The FA-functionalized nanocubes had a high sorting efficiency (S_e) and were specific for their target, since the amount of collected cells was higher compared to the cell fraction recovered using nanocubes functionalized with only PEG. Noteworthy, the annealing process did not impair the activity of the biomolecule bound to the nanocubes surface. Moreover, the results coming from the sorting experiments were confirmed also by the quantification of iron associated to the cells via elemental analysis (pg_{Fe}/cell ratio more than twice higher for csNCs_PEG-FA compared to csNCs_PEG). In addition, it was found that just 20% of the total iron used for the sorting experiment actively participated to the cells isolation. Then, it is possible to plan to reduce the amount of nanocubes used for the sorting while maintaining unaltered the efficacy in collecting cells. Despite this, also the functionalization efficiency has to be taken into account. Indeed, it is reasonable to think that a decrease of the amount of nanocubes in solution would results in a decrease of the cell-binding ability and thus retention on the column, independently from the amount of iron used. Improvement of the functionalization strategy has to flank the improvement of the sorting protocol. Besides the iron amount more parameters must be considered. These considerations can be translated also for the MNBs-based system developed and presented in chapter 1. By comparing the results on sorting when using single particles or clusters (MNBs) developed with that shown in chapter 1, it is clear that both single and clustered nanocubes are suitable for cell sorting purposes. The better sorting efficiency of single cubes than clusters can appear counterintuitive since one can expect a better magnetic response in case of nanobeads. However, this result might be explained with the local concentration effect that cells exercise by binding a large amount

of single nanocubes on the membrane. A higher amount of nanocubes associated to the cell would increase the magnetic moment of the whole system cell-nanocubes, resulting in a sorting efficiency comparable to that obtained for magnetic nanobeads. Further development of the project aims to apply the here developed nanocubes for the sorting of more relevant cancer cell lines, like ovarian cancer cells in ascites. In parallel, hyperthermia treatment should be explored, in order to extend the applicability of the system.

2.4 Materials and methods

Nanocubes synthesis

In a typical synthesis to obtain 18 nm nanocubes, 5 mL (0.015 mmol) ODE, 1.98 g (7 mmol) OLAC and 0.91 g (3 mmol) sodium oleate were added into a 50 mL three neck glass flask. Afterwards, the mixture was degassed at 110 °C for ~ca.1 h until no further bubbling was observed. The mixture was cooled to 60 °C and then 400 µL (3 mmol) $Fe(CO)_5$ dissolved in 1 mL ODE, freshly prepared in glove box, was injected into the flask. The iron precursor injection and the growth steps were carried out under nitrogen flow. The resultant yellowish mixture was heated up to 320 °C within 25 min. The mixture firstly turned to dark orange and eventually after 1 h to black, indicating the nucleation of initial crystallites. From the time of the nucleation, the mixture was kept at this temperature for additional 90 min. After cooling the obtained black suspension to 80 °C, 40 mL of chloroform was added to efficiently disperse the particles and then it was immediately cooled to room temperature (RT). The particles were precipitated by adding a 1:2 methanol/acetone solution and collected by centrifugation at 6000 rpm for 10 minutes. The precipitated particles were redissolved in fresh chloroform and the centrifuging steps were repeated five times to obtain thoroughly clean particles. Finally, the particles were readily dispersed in 40 mL chloroform and kept in glove box. The concentration of Fe was determined by ICP analysis.

Polymer coating on single nanoparticles

Polymer coating on single nanoparticles (PC-NP) was obtained using the following established method.[16, 17] The procedure is based on the coating of single nanoparticles with an amphiphilic polymer, poly(maleic anhydride-*alt*-1-octadecene). The hydrophobic side-chains of the polymer intercalate into the alkyl chains of the pristine NC`s ligand while the hydrophilic maleic anhydrides are exposed to the water phase, thus solubilizing the hydrophobic nanoparticles in polar media. To ensure a single particle polymer coating it is crucial to use an excess of polymer monomer, fixed at 500 monomer unit of polymer per nm^2 of nanoparticle surface, as already reported by our previous works.[16, 17] CcsNCs were mixed with an excess of 500 monomer/nm^2 of poly(maleic anhydride-*alt*-octadecene) in $CHCl_3$. Then, the solvent evaporation was carried out on a rotavapor. The applied vacuum was slowly decrease until a minimum of 600 mbar. The entire evaporation step took 5 h. In this step the slow evaporation of the solvent is crucial. After the complete evaporation of chloroform, borate buffer was added and the mixture sonicated for 2 h at 50 °C. Nanocubes were concentrated using an amicon centrifuge filter and separated from the excess of polymer by ultracentrifugation, using a discontinuous sucrose gradient with the following composition (sucrose : water v%): 20%, 40% and 60%, layered from the top to the bottom of the ultracentrifuge tube. After 45 min centrifugation at a speed of 25,000 rpm, the nanocubes were collected in the middle fraction, while the free polymer remained in the top layer of the gradient. The recovered nanoparticles were washed several times in order to remove the excess of sucrose. Dynamic light scattering DLS, gel electrophoresis and transmission electron microscopy (TEM) characterizations were performed to ensure that the NPs were obtained in a single, stable and not aggregated state and free from the excess of polymer.

csNCs functionalization with PEG-FA

0.1 μM of csNCs, dissolved in 500 μL of a mixture 1:3 of borate buffer (pH=9) and water, were incubated for 10 min with 12 mM of EDC (128,000 molecules per iron nanoparticle). Then, 0.55 mM of amine-PEG-FA (Mn= 2000 g/mol) (5,500 molecules per iron nanoparticle) was added and the mixture let to react for 4 h. Nanocubes were subsequently cleaned from the excess of the reagents five times in PBS buffer by centrifugation for 12 minutes at 2,800 rpm, using amicon (cutoff 100,000 g/mol).

Characterization of csNCs: DLS and gel electrophoresis

The particle hydrodynamic size distribution and zeta potential were measured using a Malvern Zetasizer operated in the 173° backscattered mode on highly diluted aqueous solution of nanocubes. The measurements were performed at 20 °C. Dynamic light scattering analysis (DLS) calculates the hydrodynamic diameter (dh) of particles in colloidal solution, giving information about homogeneity and stability of the nanoparticles in suspension. Moreover, the software of the instrument also provides a polydispersity index (PDI), which furnishes indication of the solution monodispersity. Lower is the PDI value, higher the homogeneity of the solution. Consequently, lower is the tendency to aggregation of the nanoparticle sample. In addition to the hydrodynamic size, the same instrument can also perform the zeta potential (ZP) measurements related to the surface charge of nanoparticles. This kind of analysis can give important information about the nanoparticles' surface properties such as the presence of charged groups from specific functionalizations as well as it can be used to infer about their stability in different solutions. Gel electrophoresis allows to observe the migration of the nanoparticles inside a solid agarose matrix, under the application of an electric field. The negatively-charged nanocubes migrate toward the anode indicating that the particles are single and stable, otherwise no migration should be visible. Moreover, with this technique it is also possible to exclude the presence of free polymer in solution. Indeed, if an excess of polymer is still present after the ultracentifugation step, the polymer would migrate with a different speed than the nanoparticles on the agarose gel and could be detected using UV irradiation showing a slight blue fluorescence due to the presence of the maleic anhydride ring. Gel electrophoresis was run on 1%-2% agarose gel at a voltage of 100 V for 1 h. This technique was used just for single nanocubes.

Calorimetric measurements of the specific absorption rate (SAR)

Magnetic hyperthermia studies on nanocubes were carried out using a nanoScale DM1 Series (Biomagnetics Corp.). Alternating magnetic field with a frequency of 111 kHz and 301 kHz and with a magnetic field amplitudes of 12, 15, 20 and 24 kAm^{-1} was used. The sample concentration was kept at 2 g/L and 1 g/L for the viscosity studies. The Specific Absorption Rate (SAR) value was determined by measuring the initial slope of the temperature vs. time curve (within the first seconds). The measurements are normalized to the concentration of iron taking into account the water heat capacity. All the reported SAR values and error bars were calculated from the mean and standard deviation of at least three experimental measurements. SAR values were calculated according to the following equation:

$$SAR = \left(\frac{W}{g}\right) = \frac{C}{m}\ x\ \frac{dT}{dt} \qquad (2)$$

where C is the specific heat capacity of the solvent (C_{water} = 4,185 J L^{-1} K^{-1}; $C_{gly36\%}$ = 3,550 J L^{-1} K^{-1}; $C_{gly68\%}$ = 2,850 J L^{-1} K^{-1}; $C_{gly81\%}$ = 2,580 J L^{-1} K^{-1}) and m is the concentration (g L^{-1} of Fe) of magnetic material in solution. Note that the final values are reported as (W/g_{Fe}). The measurements were carried out in non-adiabatic conditions, thus the slope of the curve dT/dt was measured by taking into account only the first few seconds (usually the slope recorded in 10 seconds) of the curve.[22]

Low-resolution Transmission electron microscopy (TEM)

Low-resolution TEM micrographs were taken using a JEOL JEM-1011 microscope operating at 100 kV. The samples were prepared by drying a drop of diluted particle suspensions on 400 mesh ultra-thin carbon coated TEM copper grids. The particle size distribution was analyzed using the automatic particle size analysis routine of ImageJ software on a low magnified TEM micrograph.

X-Ray Diffraction analysis

Powder X-ray diffraction (XRD) analysis was conducted on a Rigaku SmartLab diffractometer machine operating at 150 mA and 40 kV. The patterns were acquired in Bragg-Brentano configuration using D-tex Ultra 1D detector in the reflection mode. The samples were prepared by drop casting of concentrated particle suspensions on a zero diffraction silicon wafer. The amount of wuestite (w/w%) was determined using a semi-quantitative line profile fitting.

Cell sorting and counting

$5x10^5$ KB cells were incubated at 4 °C for 1 h with 10 µg (referred to the iron content) of csNCs, keeping a ratio of 1 µg/50,000 cells. After the incubation, the cells were centrifuged for 5 minutes at 1,000 rpm in order to remove the excess of beads, which remained in the supernatant, from the suspension. Then, the cells were magnetically sorted using MACS® MS column (Miltenyi Biotech). An excluded volume, three washes and a collected fraction were recovered. The cells were counted using NucleoCounter® NC-100™ (ChemoMetec). The same volume of cells, Reagent A100 (lysis buffer) and Reagent B (stabilizing buffer) were added to the test tube for the total cell count (cells/mL). The sorting efficiency (S_e) was calculated as percentage of the amount of the collected cells compared to the total amount of cells initially incubated with the nanocubes, according to the following equation:

$$S_e = \frac{500{,}000-(CC)}{500{,}000} \text{ x } 100 \qquad (3)$$

ICP-AES analysis of Fe

Cells samples incubated with csNCs were counted and digested with 250 µL of a concentrated H_2O_2/HNO_3 (1/2) solution for 3 h in a hot bath at 55 °C, under sonication (in order to ensure the complete digestion of the cells components). After this step, which led to the complete evaporation of H_2O_2, concentrated HCl was added (3/1 volume ratio respect to HNO_3) to reach a final volume of 500 µL. The digestion proceeded overnight at room temperature. The solution was then diluted to 5 mL with milliQ water and filtered with a PVDF filter (0.45 um) before the analysis. The intracellular Fe concentration was measured by inductively coupled plasma atomic emission spectrometry (ICP-AES, Thermofisher ICAP 6300 duo) and with the preparation of a Fe calibration curve (0.01 - 10 ppm).

2.5 References

1. Ovejero, J.G., et al., *Effects of inter- and intra-aggregate magnetic dipolar interactions on the magnetic heating efficiency of iron oxide nanoparticles.* Phys Chem Chem Phys, 2016. **18**(16): p. 10954-63.
2. Wu, W., Q.G. He, and C.Z. Jiang, *Magnetic Iron Oxide Nanoparticles: Synthesis and Surface Functionalization Strategies.* Nanoscale Research Letters, 2008. **3**(11): p. 397-415.
3. Coral, D.F., et al., *Effect of Nanoclustering and Dipolar Interactions in Heat Generation for Magnetic Hyperthermia.* Langmuir, 2016. **32**(5): p. 1201-13.
4. Guibert, C., et al., *Hyperthermia of Magnetic Nanoparticles: Experimental Study of the Role of Aggregation.* Journal of Physical Chemistry C, 2015. **119**(50): p. 28148-28154.
5. Lak, A., et al., *Size dependent structural and magnetic properties of FeO-Fe3O4 nanoparticles.* Nanoscale, 2013. **5**(24): p. 12286-12295.
6. Walter, A., et al., *Mastering the Shape and Composition of Dendronized Iron Oxide Nanoparticles To Tailor Magnetic Resonance Imaging and Hyperthermia.* Chemistry of Materials, 2014. **26**(18): p. 5252-5264.
7. Wetterskog, E., et al., *Anomalous magnetic properties of nanoparticles arising from defect structures: topotaxial oxidation of Fe(1-x)O|Fe(3-delta)O4 core|shell nanocubes to single-phase particles.* ACS Nano, 2013. **7**(8): p. 7132-44.
8. Hufschmid, R., et al., *Synthesis of phase-pure and monodisperse iron oxide nanoparticles by thermal decomposition.* Nanoscale, 2015. **7**(25): p. 11142-11154.
9. Chen, R., et al., *High-Performance Ferrite Nanoparticles through Nonaqueous Redox Phase Tuning.* Nano Letters, 2016. **16**(2): p. 1345-1351.
10. Unni, M., et al., *Thermal Decomposition Synthesis of Iron Oxide Nanoparticles with Diminished Magnetic Dead Layer by Controlled Addition of Oxygen.* Acs Nano, 2017. **11**(2): p. 2284-2303.
11. Sun, X., et al., *Tuning exchange bias in core/shell FeO/Fe3O4 nanoparticles.* Nano Lett, 2012. **12**(1): p. 246-51.
12. Lak, A., et al., *Facile transformation of FeO/Fe3O4 core-shell nanocubes to Fe3O4 via magnetic stimulation.* Sci Rep, 2016. **6**: p. 33295.
13. Guardia, P., et al., *One pot synthesis of monodisperse water soluble iron oxide nanocrystals with high values of the specific absorption rate.* Journal of Materials Chemistry B, 2014. **2**(28): p. 4426-4434.
14. Lopez-Ortega, A., et al., *Topotaxial Phase Transformation in Cobalt Doped Iron Oxide Core/Shell Hard Magnetic Nanoparticles.* Chemistry of Materials, 2017. **29**(3): p. 1279-1289.
15. Di Corato, R., et al., *Water solubilization of hydrophobic nanocrystals by means of poly(maleic anhydride-alt-1-octadecene).* Journal of Materials Chemistry, 2008. **18**(17): p. 1991-1996.
16. Quarta, A., et al., *Multifunctional nanostructures based on inorganic nanoparticles and oligothiophenes and their exploitation for cellular studies.* Journal of the American Chemical Society, 2008. **130**(32): p. 10545-10555.
17. Pellegrino, T., et al., *Hydrophobic nanocrystals coated with an amphiphilic polymer shell: A general route to water soluble nanocrystals.* Nano Letters, 2004. **4**(4): p. 703-707.
18. Kumar, S., et al., *Electrostatic strengths of salt bridges in thermophilic and mesophilic glutamate dehydrogenase monomers.* Proteins-Structure Function and Genetics, 2000. **38**(4): p. 368-383.
19. Palm, T., R. Esfandiary, and R. Gandhi, *The effect of PEGylation on the stability of small therapeutic proteins.* Pharmaceutical Development and Technology, 2011. **16**(5): p. 441-448.
20. Lee, P., et al., *PEGylation to Improve Protein Stability During Melt Processing.*

Macromolecular Bioscience, 2015. **15**(10): p. 1332-1337.
21. Morgenstern, J., et al., *Effect of PEG molecular weight and PEGylation degree on the physical stability of PEGylated lysozyme.* International Journal of Pharmaceutics, 2017. **519**(1-2): p. 408-417.
22. Casula, M.F., et al., *Manganese doped-iron oxide nanoparticle clusters and their potential as agents for magnetic resonance imaging and hyperthermia.* Physical Chemistry Chemical Physics, 2016. **18**(25): p. 16848-16855.
23. Cabrera, D., et al., *Unraveling viscosity effects on the hysteresis losses of magnetic nanocubes.* Nanoscale, 2017. **9**(16): p. 5094-5101.
24. Pelaz, B., et al., *Surface Functionalization of Nanoparticles with Polyethylene Glycol: Effects on Protein Adsorption and Cellular Uptake.* ACS Nano, 2015. **9**(7): p. 6996-7008.